CHINESE OPTICS LETTERS

Vol. 21, No. 8 | August 2023

# Momentum filtering scheme of cooling atomic clouds for the Chinese Space Station

Hui Li (李 荟)[1], Biao Wu (武 彪)[1], Jiachen Yu (于佳晨)[1], Xiaolong Yuan (袁小龙)[1], Xiaoji Zhou (周小计)[1], Bin Wang (汪 斌)[2], Weibiao Chen (陈卫标)[2], Wei Xiong (熊 炜)[1*], and Xuzong Chen (陈徐宗)[1**]

[1] Institute of Quantum Electronics, School of Electronics, Peking University, Beijing 100871, China

[2] Shanghai Institute of Optics and Fine Mechanics, Chinese Academy of Sciences, Shanghai 201800, China

*Corresponding author: xiong-wei@pku.edu.cn

**Corresponding author: xuzongchen@pku.edu.cn

Received January 16, 2023 | Accepted April 25, 2023 | Posted Online August 8, 2023

To obtain cold atom samples with temperatures lower than 100 pK in the cold atom physics rack experiment of the Chinese Space Station, we propose to use the momentum filtering method for deep cooling of atoms. This paper introduces the experimental results of the momentum filtering method verified by our ground testing system. In the experiment, we designed a specific experimental sequence of standing-wave light pulses to control the temperature, atomic number, and size of the atomic cloud. The results show that the momentum filter can effectively and conveniently reduce the temperature of the atomic cloud and the energy of Bose–Einstein condensation, and can be flexibly combined with other cooling methods to enhance the cooling effect. This work provides a method for the atomic cooling scheme of the ultra-cold atomic system on the ground and on the space station, and shows a way of deep cooling atoms.

**Keywords:** momentum filter; standing-wave pulse; Bose–Einstein condensation; optical dipole trap; two-stage cooling; space station.

**DOI:** 10.3788/COL202321.080201

## 1. Introduction

Getting colder atomic temperatures through different methods has been a fascinating and challenging task. At lower temperatures, scientists can observe many wonderful physical phenomena that have not been possible in experiments before. The related exploration and research may bring breakthroughs in the field of quantum physics and precise physical measurement[1,2]. Ultra-cold quantum systems are expected to be used to measure faint physical phenomena, including gravitational waves[3-5] and testing the standard model of particle physics[6-8]. Scientific researchers in many institutions around the world are engaged in various efforts at lower temperatures. The successful preparation of Bose–Einstein condensation (BEC)[9-11] undoubtedly provides a good and effective way to achieve lower temperature in experiments. The need for experiments with higher precision and longer interference time has also led to the development of various ways to cool atoms. At present, the main methods of atomic deep cooling schemes reported are as follows: in 2003, Ketterle's team implemented two decompression cooling steps after RF evaporative cooling in a ground magnetic trap, achieving a temperature of 450 pK for atomic gas of Na[12]; in 2015, Kasevich's team used the delta-kick cooling (DKC) scheme to achieve rubidium clouds with a two-dimensional transverse temperature of 50 pK[13,14]. Further cooling requires a microgravity environment provided by the drop tower[15], parabolic aircraft[16], rocket[17], or space station[18,19]. There are two main options for deep atomic cooling in microgravity. One is the atomic-chip technique used by teams at NASA's Jet Propulsion Laboratory (JPL) and Rasel in Germany, which uses DKC or adiabatic release[15,17-24]; the other is the all-optical trap technique used by the research group of Bouyer in France and the research team of the cold atom physics rack (CAPR) on the Chinese Space Station, using a velocity-selective Raman light pulse or two-stage cooling (TSC)[16,25-31].

We have verified the feasibility and effectiveness of TSC through theoretical and ground experiments, and provided the implementation scheme and specific parameter reference for the ultra-cold atomic experiment system of the space station[25-30]. To further reduce the atomic temperature, momentum filtering is experimentally verified. Based on the principle of atomic momentum states manipulated by optical standing-wave pulse sequences[32,33], the Talbot–Lau interferometer with specific parameters is used to form the momentum filter for atom redistribution and momentum compression in momentum

space[34,35]. Moreover, we innovatively combine momentum filtering cooling with TSC. Experimental results show that the filter can cool atoms quickly and deeply, and can be flexibly combined with other cooling schemes to further reduce the temperature. In practical applications, a momentum filter can improve the measurement precision and application effect of an atomic interferometer, gyroscope, gravimeter, and other precision measuring instruments[36-39]. In this work, the momentum filtering principle is applied to reduce atomic temperature, and a series of experiments is carried out to verify it.

In this paper, the experimental system and the physical process of the experiment are introduced in detail, the method of cooling atoms by momentum filtering after TSC is demonstrated, and the results are obtained. In the experiment, the effect of momentum filtering to cool atoms after primary evaporation cooling and TSC is verified to achieve ultra-low temperatures. The optimal pulse interval time is proposed after several experiments, and the cooling scheme is proposed for the Chinese Space Station ultra-cold atomic experiments. The momentum filtering method is simple in equipment and timing, and it can be used in combination with a variety of cooling methods such as TSC or DKC, which opens up a new path for deep cooling of atoms.

## 2. Experimental System

The experimental system is a ground-based prototype that provides solution verification and technical support for the ultracold atomic experiment system CAPR on the Chinese Space Station. The alkali metal atom $^{87}$Rb was used in the experiment to prepare the BEC. As shown in Fig. 1(a), the system in vacuum consists of the rubidium atom source, two-dimensional precooling chamber, three-dimensional cooling science chamber, ion pump, and titanium sublimation pump. The vacuum pressures of the precooling chamber and science chamber are maintained at $2 \times 10^{-7}$ Pa and $5 \times 10^{-9}$ Pa, respectively. The phase locking and power amplification of cooling light, repumping light, probing light, and push light are designed and realized in the laser platform. The frequencies of each functional light in the laser cooling process are shown in Fig. 1(b). The frequency of the reference beam aligns with the $^{87}$Rb $D_2$B line ($5^2S_{1/2} \rightarrow 5^2P_{3/2}$) $F = 1 \rightarrow F' = 1$ and 2 crossover (average value of $F = 1 \rightarrow F' = 1$ and $F = 1 \rightarrow F' = 2$). The repumping light is obtained by the reference light with a shift of 78.4735 MHz at frequency $F = 1 \rightarrow F' = 2$. The cooling light has a negative detuning $\Delta$ from $F = 2 \rightarrow F' = 3$, and $\Delta$ gradually increases from $-21$ MHz to $-108$ MHz in an optical molasses process. The probing light (frequency of $F = 2 \rightarrow F' = 3$) was imaged in horizontal and vertical directions of the science chamber. After beam splitting and beam combining, these functional lights are coupled into optical fibers, through which each laser is transported to the vicinity of the vacuum chamber and acts on the atom. After the process of magneto-optical trap (MOT), molasses, and all-optical trap evaporation cooling, the BEC of $^{87}$Rb atoms in $F = 1$ state is achieved.

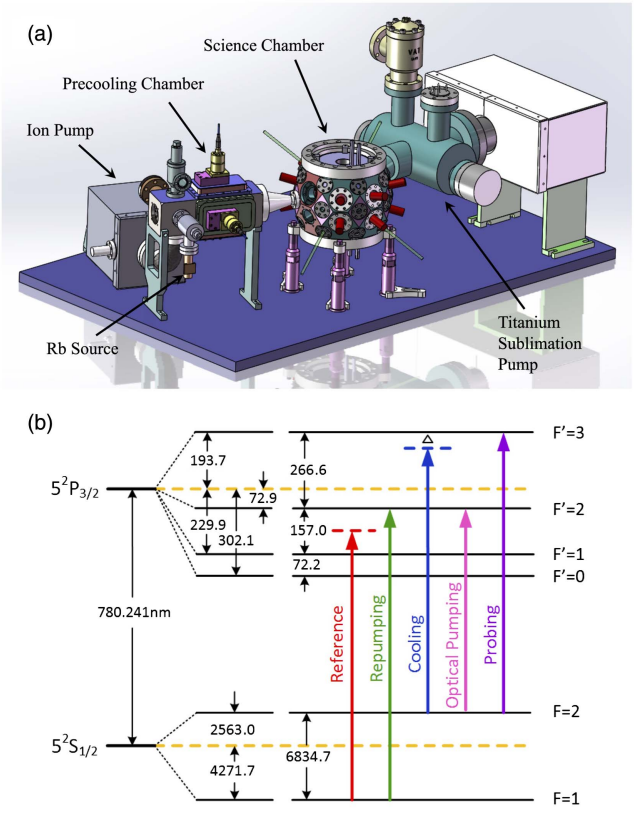


**Fig. 1.** (a) Experimental setup of atomic deep cooling, consisting of rubidium atom source, precooling chamber, science chamber, ion pump, and titanium sublimation pump. (b) Rubidium 87 $D_2$ transition hyperfine structure, with frequency of each functional light during the laser cooling of atoms.

The evaporation cooling process is completed under the action of the optical dipole trap (ODT) formed by 1064 nm fiber lasers. The beam waist width of the optical trap is 80 μm. Momentum filtering experiments were performed after BEC formation in the trap. The standing-wave laser pulses as the momentum filter come from a 1064 nm laser. The schematic diagram of the optical path of the experimental system is shown in Fig. 2, where one window of the cavity serves as the laser entry port, and a mirror is placed at the opposite window to form a standing wave. The momentum filtering light path and the imaging light share the same light path through the dichroic mirror. The output power of the pulsed laser is 1 W. First, a Kapitza–Dirac scattering experiment[40-42] was performed to determine the trap depth of the standing wave. The pulse time corresponding to the removal of atoms near the zero momentum state on the system was determined to be 1.65 μs, which is also the pulse width of our momentum filtering experiments. In the experiment, the standing-wave pulse time and pulse interval are adjusted to optimize the momentum filter.

To achieve lower temperatures, another attempt was made. We combine the momentum filtering cooling scheme with the TSC scheme[29]. The second stage applies a loosely confined optical trap, and the first stage uses a tightly confined optical trap, sharing the same crossed beam optical path. The atoms

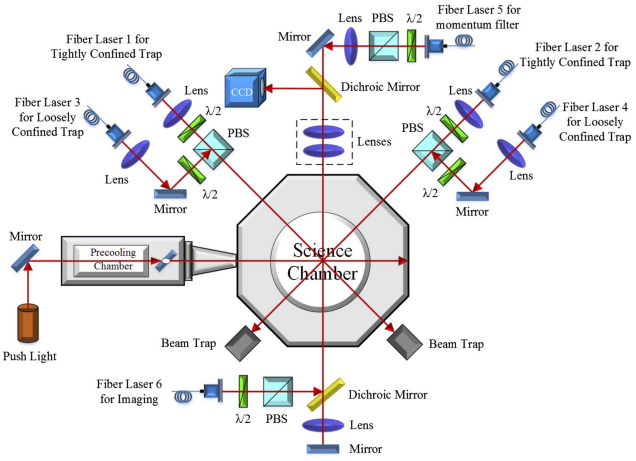


**Fig. 2.** Schematic diagram of the optical path of the experimental system. Fiber lasers 1 to 5 are 1064 nm fiber lasers. The waist width of fiber laser beams 1 and 2 is 80 μm, and the cross optical trap formed is a tightly combined trap. The width of fiber laser beams 3 and 4 is 300 μm, and the cross optical trap formed is loosely confined trap. Fiber laser 5 forms a standing wave under the adjustment of the opposite mirror. The momentum filtering pulse (fiber laser 5) and imaging light (fiber laser 6) share the same light path through the dichroic mirror.

are first adiabatically transferred from the tightly confined trap to the loosely confined trap with a waist width of 300 μm for diffusion cooling, and then momentum filtering experiments are carried out to obtain lower temperature atomic clouds. In the experiment, the laser power of the ODT evaporative cooling and TSC, and the optical pulse sequence of momentum filtering cooling are detailed in Section 4 of this paper.

## 3. Physical Process

For the Talbot–Lau interferometer, the matter wave in time domain and the light wave in space are similar. The Talbot effect occurs after the light field passes through the first grating, then phase evolves in free space, and the near-field diffraction occurs again after the light field passes through the second grating[43-47]. The Talbot–Lau interferometer for matter waves in the time domain is analogous[32-35]. The effect of both pulses of the standing-wave light field is related to the optical potential trap depth of $U_p$ and the pulse width of $\tau_p$. The two pulses behave similarly to the two gratings. Light field phase evolves in space, and matter wave phase evolves in the time interval. The characteristic Talbot time $T_{\mathrm{Talbot}} = h/E_{\mathrm{recoil}}$ is the minimum time for the phase of the material wavefront to be completely reconstructed after the first pulse, where $E_{\mathrm{recoil}}$ is the recoil energy of the atom for the laser used to generate the standing-wave pulse[33]. When the first pulse is applied, the phase evolution of the $n$th momentum state in the time interval $\tau_{\mathrm{interval}}$ is $e^{-iE^{(n)}t/\hbar}$, where $E^{(n)} = (2n\hbar k)^2/2m = 4n^2E_R$. $E_R = (\hbar k_L)^2/2m$ is the single-photon recoil energy, where $m$ is the mass of the atom, $k = 2\pi/\lambda$ is the wave vector of the laser, and $\lambda$ is the laser wavelength.

The pulse width determines the magnitude of the phase evolution of each Bloch state. The standing-wave pulse scatters the atomic gas with momentum around $0\hbar k$ onto the momentum state of $\pm 2n\hbar k$ $(n = 0, 1, 2\ldots)$. When the phase evolution time of the matter wave is an integer multiple of Talbot time, the difference between the phase of the wavefront and the initial matter wave is an integer multiple of $2\pi$. This means that the state of the atom before the second pulse is the same as the state after the first pulse. When the phase evolution time of the matter wave is an odd-number multiple of half Talbot time, the action of two optical lattice pulses can achieve coherent cancellation if the matter wave is considered as a monochromatic plane wave. Such a designed Talbot–Lau interferometer with a specific pulse intensity and pulse time interval formed by standing waves acts on the atomic gas, and the momentum filtering effect appears.

Figure 3 shows the schematic diagram of the physical process of cooling atoms in the experiment with momentum filtering. When the pulse interval is an odd-number multiple of $T_{\mathrm{Talbot}}/2 = \pi\hbar/4E_R \approx 61.5\,\mu\mathrm{s}$, the phase evolution of adjacent momentum states differs by an odd-number multiple of $\pi$. Before the second pulse acts on atoms, the interference of each momentum state reaches a maximum of coherent cancellation. The second pulse and first pulse have completely opposite effects on the atom and cancel each other out. So the atoms end up mostly in the same momentum state as they were before scattering. In this way, the atoms with higher temperatures and lower temperatures are separated, so as to achieve the effect of narrowing the momentum width and reducing the cold atomic cloud temperature of the observation system.

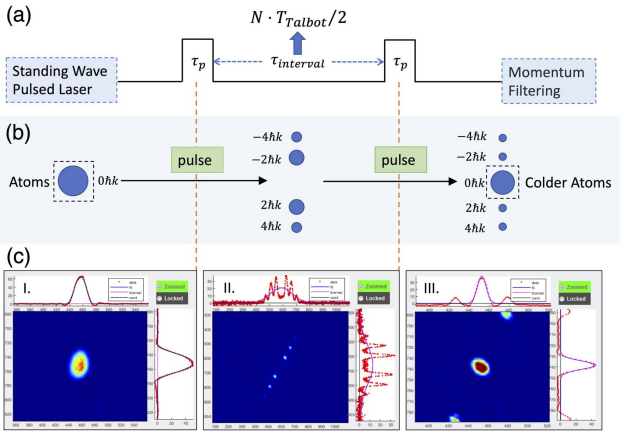


**Fig. 3.** Schematic diagram of the physical process of cooling atoms in the experiment with momentum filtering. (a) Standing-wave pulse sequence with momentum filtering cooling effect, pulse width $\tau_p$ = 1.65 μs, pulse time interval $\tau_{\mathrm{interval}} = N \cdot T_{\mathrm{Talbot}}/2$ ($N$ = 1, 3, 5 . . . ). (b) After the first pulse, an atomic cloud around $0\hbar k$ is scattered to the momentum state of $\pm 2n\hbar k$ ($n$ = 0, 1, 2 . . . ); after the second pulse, atoms are scattered back to the initial momentum state. Atoms with high temperatures are removed from the cloud, resulting in colder atoms. (c) Experimental images of atoms corresponding to the momentum filtering process.

## 4. Results and Analysis

During the evaporation cooling stage of the first tightly confined ODT, fiber lasers 1 and 2 in Fig. 2 are turned on to form a cross beam with the waist width of 80 μm. The power of a single laser is gradually reduced from 5 W to 23 mW with an exponential curve, and the whole process takes 5700 ms. In this case, the atomic number of BEC is $5.14 \times 10^4$, and the temperature is 30.8 nK (time of flight TOF = 20 ms). Momentum filtering cooling was performed after ODT, and fiber laser 5 was turned on and pulsed according to the sequence shown in Fig. 3. Both pulses had a width of 1.65 μs and a consistent intensity of 1 W. In the experiment, multiple groups of experiments were carried out with pulse intervals of 1, 3, 5, 7, and 9 times $T_{\text{Talbot}}/2$. The temperature and atomic number of the BEC after momentum filtering were probed with TOF = 20 ms, and the experimental results under different settings are shown in Fig. 4 with blue markers. The temperatures of atomic clouds corresponding to the five pulse intervals are 17.2 nK, 8.7 nK, 6.5 nK, 5.9 nK, and 6.4 nK, and the number of atoms is $3.10 \times 10^4$, $1.34 \times 10^4$, $8.26 \times 10^3$, $8.72 \times 10^3$, and $6.13 \times 10^3$, respectively.

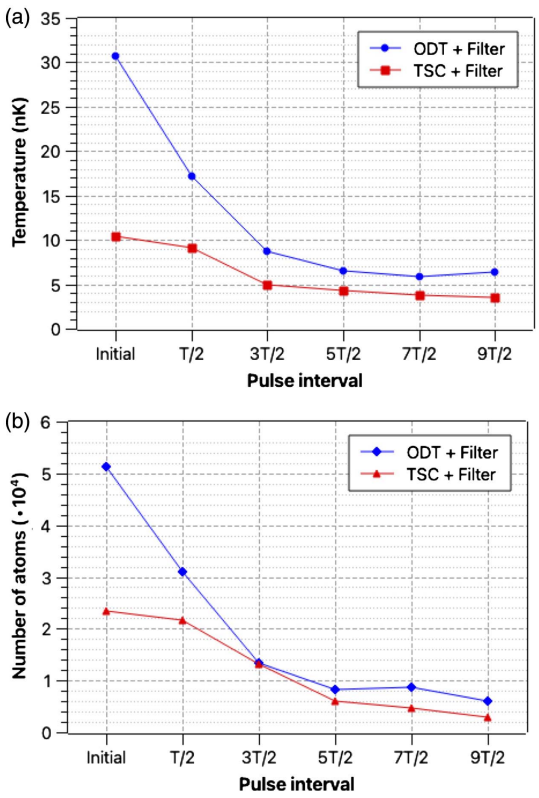


**Fig. 4.** (a) Temperature of atomic clouds at different momentum filtering pulse intervals. (b) Number of atoms at different pulse intervals. For both (a) and (b), $T$ on the horizontal axis represents $T_{\text{Talbot}}$, and initial denotes the BEC state before performing momentum filtering. Blue symbols are the experimental results of momentum filtering implemented after evaporative cooling of the first stage tightly confined optical dipole trap. Red symbols show the experimental results of momentum filtering implemented after two-stage cooling.

Compared with the initial experimental results of ODT evaporation cooling, the cooling effect of momentum filtering can be clearly seen, and the momentum width of atomic clouds is reduced.

To further cool the atoms and verify the combination effect with other cooling schemes, we implemented a combination of TSC and momentum filtering cooling schemes. The BEC prepared by the first ODT was adiabatically transferred to the second loosely confined trap with the beam waist width of 300 μm. The power of fiber lasers 3 and 4 increased slowly to 200 mW at the end of the first evaporative cooling stage, held for 50 ms, and then gradually reduced to 74 mW with an exponential curve. The number of atoms of the BEC after TSC is $2.34 \times 10^4$, and the temperature is 10.4 nK (TOF = 20 ms). Momentum filtering cooling is subsequently superimposed on the atoms. The pulse width, pulse intensity, and pulse interval of the standing-wave lasers are set to be the same as above. The corresponding atomic cloud temperatures in the case of five pulse intervals are obtained as follows: 9.1 nK, 4.9 nK, 4.3 nK, 3.8 nK, and 3.5 nK, and the number of atoms is $2.17 \times 10^4$, $1.31 \times 10^4$, $5.93 \times 10^3$, $4.60 \times 10^3$, and $2.81 \times 10^3$ respectively. The experimental results are shown in Fig. 4 with red markers. The cooling effect of momentum filtering is obvious, and applying momentum filters after other cooling schemes can further reduce the momentum width of BEC atomic clouds.

Comparing all experimental results, the state of the BEC is best when the TSC is combined with the momentum filtering scheme with the pulse interval of $3T_{\text{Talbot}}/2$. The temperature of atomic cloud is 4.9 nK, the number of atoms is $1.31 \times 10^4$, and the radius of the atomic cloud is 18.3 μm in the $x$ direction and 20.8 μm in the $y$ direction (TOF = 20 ms). To further analyze and research the atomic cloud under this experimental condition, the BEC states were probed at different TOFs in the experiment. The temperature, number of atoms, and size of the atomic cloud (characterized by the average radius of the atomic cloud in $x$ and $y$ directions) of the BEC were probed at TOFs of 15 ms, 20 ms, 25 ms, 30 ms, and 35 ms, respectively. The experimental results and BEC images under different TOFs are shown in Fig. 5. According to the experimental data, the size of the atomic cloud increases linearly with the TOF, and the variance of the temperature of BEC measured at different TOFs is 0.12. The maximum number of atoms is probed when TOF is 20 ms. The scheme of momentum filtering with a standing-wave pulse interval of $3T_{\text{Talbot}}/2$ combined with TSC can be considered as a better way to cool atoms in this experimental system. The detection results with the TOF of 20 ms are also representative.

The temperature obtained by the momentum filter is theoretically inversely proportional to the interval time between two pulses[35]. Increasing the pulse interval time can further reduce the temperature, but on the other hand, it will increase the loss of atomic number. In the ground experiment, the atoms will deviate from the pulse area due to the influence of gravity. In microgravity, the pulse interval time can be further increased to obtain even lower temperatures. On the space station, there is no need

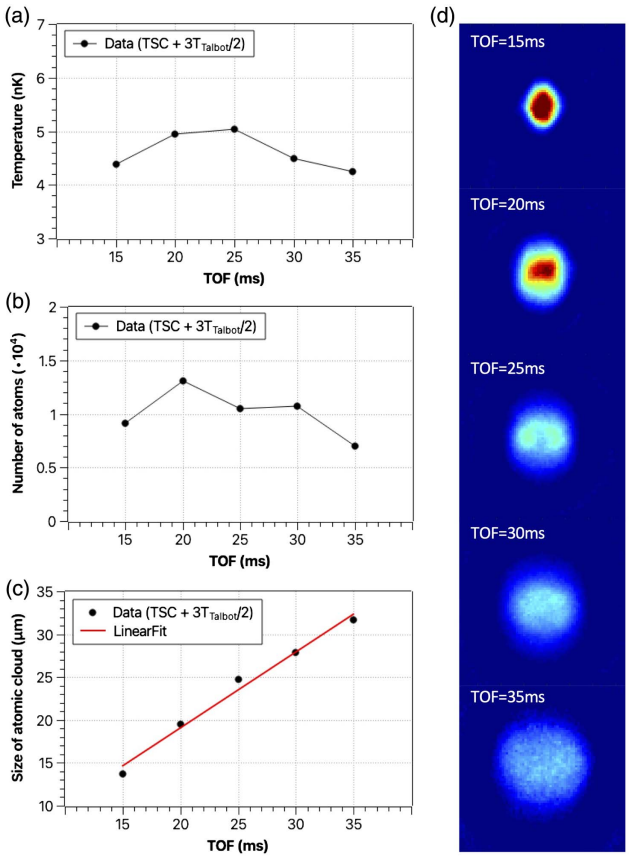


**Fig. 5.** Experimental results of the combination of two-stage cooling and momentum filtering with the pulse interval of $3T_{Talbot}/2$ at different TOFs: (a) temperature of atomic cloud, (b) number of atoms, (c) size of atomic cloud, and (d) images of BEC.

to add the magnetic field gradient to compensate for gravity, and the minimum temperature of atoms is not limited by the ground state energy of the potential well.

The experimental results demonstrate that the momentum filtering cooling scheme is feasible and effective. In the space station experiment, all the optical mechanical parts of the on-orbit CAPR are specially designed and fixed on the cavity, and all laser transmission is completed through optical fibers. The modification of the pulse sequence requires only the input of parameters in the control system on the computer. The momentum filtering cooling scheme is easy to implement and control, and its flexibility and reliability can be guaranteed.

## 5. Conclusion

This paper introduces the experimental results of the momentum filtering method for atomic cooling on the ground prototype of CAPR on the Chinese Space Station. We describe the experimental system of BEC preparation and the momentum filter cooling scheme in detail. By designing a specific pulse width and different standing-wave pulse intervals, combined with other deep cooling schemes, the effectiveness and flexibility of momentum filtering as an atomic cooling scheme are confirmed. The best pulse sequence of momentum filtering cooling is obtained on this system, which provides reference and experimental data support for the deep cooling scheme of the space station on-orbit experimental system. The feasibility of applying a momentum filter to cool atoms in CAPR of the Chinese Space Station is verified. Moreover, this work provides a method for cooling atoms and reducing the momentum width of BEC on the ground cold atom platform. We achieve an atomic cloud below 4 nK on the ground using the scheme of momentum filtering combined with TSC. The temperature of the atomic cloud can be further reduced in microgravity. The momentum filter is simple and easy to manipulate and implement. The platform with the experimental conditions of a standing-wave pulse or optical lattice can use this scheme to further cool the atomic cloud. At the same time, it can be combined with other cooling methods to further strengthen the cooling effect.

## Acknowledgement

This work was supported by the National Natural Science Foundation of China (Nos. 11920101004 and 11934002) and the National Key Research and Development Program of China (Nos. 2021YFA1400900 and 2021YFA0718300).

## References

1. I. Bloch, J. Dalibard, and S. Nascimbène, "Quantum simulations with ultracold quantum gases," Nat. Phys. **8**, 267 (2012).
2. G. Rosi, F. Sorrentino, L. Cacciapuoti, M. Prevedelli, and G. M. Tino, "Precision measurement of the Newtonian gravitational constant using cold atoms," Nature **510**, 518 (2014).
3. J. M. Hogan, D. M. S. Johnson, S. Dickerson, T. Kovachy, A. Sugarbaker, S. W. Chiow, P. W. Graham, M. A. Kasevich, B. Saif, S. Rajendran, P. Bouyer, B. D. Seery, L. Feinberg, and R. Keski-Kuha, "An atomic gravitational wave interferometric sensor in low Earth orbit (AGIS-LEO)," Gen. Relativ. Gravit. **43**, 1953 (2011).
4. P. W. Graham, J. M. Hogan, M. A. Kasevich, and S. Rajendran, "New method for gravitational wave detection with atomic sensors," Phys. Rev. Lett. **110**, 171102 (2013).
5. S. Dimopoulos, P. W. Graham, J. M. Hogan, M. A. Kasevich, and S. Rajendran, "Gravitational wave detection with atom interferometry," Phys. Lett. B **678**, 37 (2009).
6. M. Endres, T. Fukuhara, D. Pekker, M. Cheneau, P. Schauß, C. Gross, E. Demler, S. Kuhr, and I. Bloch, "The 'Higgs' amplitude mode at the two-dimensional superfluid/Mott insulator transition," Nature **487**, 454 (2012).
7. J. Léonard, A. Morales, P. Zupancic, T. Donner, and T. Esslinger, "Monitoring and manipulating Higgs and Goldstone modes in a supersolid quantum gas," Science **358**, 1415 (2017).
8. M. Di Liberto, A. Recati, N. Trivedi, I. Carusotto, and C. Menotti, "Particle-hole character of the Higgs and goldstone modes in strongly interacting lattice bosons," Phys. Rev. Lett. **120**, 073201 (2018).
9. M. H. Anderson, J. R. Ensher, M. R. Matthews, C. E. Wieman, and E. A. Cornell, "Observation of Bose-Einstein condensation in a dilute atomic vapor," Science **269**, 198 (1995).
10. K. B. Davis, M. O. Mewes, M. R. Andrews, N. J. van Druten, D. S. Durfee, D. M. Kurn, and W. Ketterle, "Bose-Einstein condensation in a gas of sodium atoms," Phys. Rev. Lett. **75**, 3969 (1995).
11. C. C. Bradley, C. A. Sackett, J. J. Tollett, and R. G. Hulet, "Evidence of Bose-Einstein condensation in an atomic gas with attractive interactions," Phys. Rev. Lett. **75**, 1687 (1995).

12. A. E. Leanhardt, T. A. Pasquini, M. Saba, A. Schirotzek, Y. Shin, D. Kielpinski, D. E. Pritchard, and W. Ketterle, "Cooling Bose-Einstein condensates below 500 picokelvin," Science **301**, 1513 (2003).
13. H. Ammann and N. Christensen, "Delta kick cooling: a new method for cooling atoms," Phys. Rev. Lett. **78**, 2088 (1997).
14. T. Kovachy, J. M. Hogan, A. Sugarbaker, S. M. Dickerson, C. A. Donnelly, C. Overstreet, and M. A. Kasevich, "Matter wave lensing to picokelvin temperatures," Phys. Rev. Lett. **114**, 143004 (2015).
15. T. Van Zoest, N. Gaaloul, Y. Singh, H. Ahlers, W. Herr, S. T. Seidel, E. Rasel, T. Hänsch, and J. Reichel, "Bose-Einstein condensation in microgravity," Science **328**, 1540 (2010).
16. R. Geiger, V. Ménoret, G. Stern, N. Zahzam, P. Cheinet, B. Battelier, and P. Bouyer, "Detecting inertial effects with airborne matter-wave interferometry," Nat. Commun. **2**, 474 (2011).
17. D. Becker, M. D. Lachmann, S. T. Seidel, H. Ahlers, A. N. Dinkelaker, J. Grosse, and E. Rasel, "Space-borne Bose-Einstein condensation for precision interferometry," Nature **562**, 391 (2018).
18. E. Gibney, "Universe's coolest lab set to open up quantum world," Nature **557**, 151 (2018).
19. D. C. Aveline, J. R. Williams, E. R. Elliott, C. Dutenhoffer, J. R. Kellogg, J. M. Kohel, N. E. Lay, K. Oudrhiri, R. F. Shotwell, N. Yu, and R. J. Thompson, "Observation of Bose–Einstein condensates in an Earth-orbiting research lab," Nature **582**, 193 (2020).
20. A. Cho, "Trapped in orbit," Science **357**, 986 (2017).
21. C. A. Sackett, T. C. Lam, J. C. Stickney, and J. H. Burke, "Extreme adiabatic expansion in micro-gravity: modeling for the cold atomic laboratory," Microgravity Sci. Technol. **30**, 155 (2018).
22. E. R. Elliott, M. C. Krutzik, J. R. Williams, R. J. Thompson, and D. C. Aveline, "NASA's Cold Atom Lab (CAL): system development and ground test status," NPJ Microgravity **4**, 16 (2018).
23. R. Corgier, S. Amri, W. Herr, H. Ahlers, J. Rudolph, D. Guéry-Odelin, E. Rasel, and N. Gaaloul, "Fast manipulation of Bose–Einstein condensates with an atom chip," New J. Phys. **20**, 055002 (2018).
24. H. Müntinga, H. Ahlers, M. Krutzik, A. Wenzlawski, S. Arnold, D. Becker, and E. Rasel, "Interferometry with Bose-Einstein condensates in microgravity," Phys. Rev. Lett. **110**, 093602 (2013).
25. L. Wang, P. Zhang, X. Chen, and Z. Ma, "Generating a picokelvin ultracold atomic ensemble in microgravity," J. Phys. B **46**, 195302 (2013).
26. H. Yao, T. Luan, C. Li, Y. Zhang, Z. Ma, and X. Chen, "Comparison of different techniques in optical trap for generating picokelvin 3D atom cloud in microgravity," Opt. Commun. **359**, 123 (2016).
27. T. Luan, Y. Li, X. Zhang, and X. Chen, "Realization of two-stage crossed beam cooling and the comparison with delta-kick cooling in experiment," Rev. Sci. Instrum. **89**, 123110 (2018).
28. B. Fan, L. Zhao, Y. Zhang, J. Sun, W. Xiong, J. Chen, and X. Chen, "Numerical study of evaporative cooling in the space station," J. Phys. B **54**, 015302 (2020).
29. H. Li, J. Yu, X. Yuan, B. Wu, Y. Xie, L. Li, A. Liang, M. Huang, S. Jin, W. Xiong, B. Wang, D. Chen, T. Li, X. Hou, L. Li, X. Zhou, W. Chen, and X. Chen, "Deep cooling scheme of quantum degenerate gas and ground experimental verification for Chinese Space Station," Front. Phys. **10**, 971059 (2022).
30. Y. Xie, B. Fan, H. Li, A. Liang, M. Huang, B. Wu, B. Wang, X. Chen, and L. Liu, "Ground experiment verification and on-orbit prediction of the two-stage cooling at pK level in the Chinese Space Station," J. Phys. B **55**, 205301 (2022).
31. X. Chen and B. Fan, "The emergence of picokelvin physics," Rep. Prog. Phys. **83**, 076401 (2020).
32. L. Deng, E. W. Hagley, J. Denschlag, J. E. Simsarian, M. Edwards, C. W. Clark, K. Helmerson, S. L. Rolston, and W. D. Phillips, "Temporal, matter-wave-dispersion talbot effect," Phys. Rev. Lett. **83**, 5407 (1999).
33. M. Edwards, B. Benton, J. Heward, and C. W. Clark, "Momentum-space engineering of gaseous Bose-Einstein condensates," Phys. Rev. A **82**, 063613 (2010).
34. W. Xiong, X. Yue, Z. Wang, X. Zhou, and X. Chen, "Manipulating the momentum state of a condensate by sequences of standing-wave pulses," Phys. Rev. A **84**, 043616 (2011).
35. W. Xiong, X. Zhou, X. Yue, Y. Zhai, and X. Chen, "A momentum filter for atomic gas," New J. Phys. **15**, 063025 (2013).
36. J. P. Dowling, "Correlated input-port, matter-wave interferometer: quantum-noise limits to the atom-laser gyroscope," Phys. Rev. A **57**, 4736 (1998).
37. K. Eckert, P. Hyllus, D. Bruß, U. V. Poulsen, M. Lewenstein, C. Jentsch, T. Müller, E. M. Rasel, and W. Ertmer, "Differential atom interferometry beyond the standard quantum limit," Phys. Rev. A **73**, 013814 (2006).
38. V. Ménoret, P. Vermeulen, N. Le Moigne, S. Bonvalot, P. Bouyer, A. Landragin, and B. Desruelle, "Gravity measurements below $10^{-9}$ g with a transportable absolute quantum gravimeter," Sci. Rep. **8**, 12300 (2018).
39. S. Gupta, K. Dieckmann, Z. Hadzibabic, and D. E. Pritchard, "Contrast interferometry using Bose-Einstein condensates to measure $h/m$ and $\alpha$," Phys. Rev. Lett. **89**, 140401 (2002).
40. P. L. Gould, G. A. Ruff, and D. E. Pritchard, "Diffraction of atoms by light: the near-resonant Kapitza-Dirac effect," Phys. Rev. Lett. **56**, 827 (1986).
41. E. M. Rasel, M. K. Oberthaler, H. Batelaan, J. Schmiedmayer, and A. Zeilinger, "Atom wave interferometry with diffraction gratings of light," Phys. Rev. Lett. **75**, 2633 (1995).
42. A. D. Cronin, J. Schmiedmayer, and D. E. Pritchard, "Optics and interferometry with atoms and molecules," Rev. Mod. Phys. **81**, 1051 (2009).
43. J. F. Clauser and M. W. Reinsch, "New theoretical and experimental results in Fresnel optics with applications to matter-wave and x-ray interferometry," Appl. Phys. B **54**, 380 (1992).
44. J. F. Clauser and S. Li, "Talbot-von Lau atom interferometry with cold slow potassium," Phys. Rev. A **49**, R2213 (1994).
45. M. S. Chapman, C. R. Ekstrom, T. D. Hammond, J. Schmiedmayer, B. E. Tannian, S. Wehinger, and D. E. Pritchard, "Near-field imaging of atom diffraction gratings: the atomic Talbot effect," Phys. Rev. A **51**, R14 (1995).
46. S. Nowak, Ch. Kurtsiefer, T. Pfau, and C. David, "High-order Talbot fringes for atomic matter waves," Opt. Lett. **22**, 1430 (1997).
47. W. B. Case, M. Tomandl, S. Deachapunya, and M. Arndt, "Realization of optical carpets in the Talbot and Talbot-Lau configurations," Opt. Express **17**, 020966 (2009).